ARTICLE NO. 79-4081

Sound Production Due to Large-Scale Coherent Structures

Thomas B. Gatski*
NASA Langley Research Center, Hampton, Va.

The acoustic pressure fluctuations due to large-scale finite amplitude disturbances in a free turbulent shear flow are calculated. The flow is decomposed into three component scales: the mean motion, the large-scale wave-like disturbance, and the small-scale random turbulence. The effect of the large-scale structure on the flow is isolated by applying both a spatial and phase average on the governing differential equations and by initially taking the small-scale turbulence to be in energetic equilibrium with the mean flow. The subsequent temporal evolution of the flow is computed from global energetic rate equations for the different component scales. Lighthill's theory is then applied to the region with the flowfield as the source and an observer located outside the flowfield in a region of uniform velocity. Since the time history of all flow variables is known, a minimum of simplifying assumptions for the Lighthill stress tensor is required, including no far-field approximations. A phase average is used to isolate the pressure fluctuations due to the large-scale structure, and also to isolate the dynamic process responsible. Variation of mean square pressure with distance from the source is computed to determine the acoustic far-field location and decay rate, and, in addition, spectra at various acoustic field locations are computed and analyzed. Also included are the effects of varying the growth and decay of the large-scale disturbance on the sound produced.

I. Introduction

THE presence of large-scale coherent structures in turbulent shear flows and their role in the sound generation process have been the impetus for many recent scientific studies. At present, both the acoustician and fluid dynamicist are interested in these structures—the acoustician to understand the mechanisms responsible for the sound with a view toward its subsequent suppression, and the fluid dynamicist to understand the structure of turbulent flows.

For example, the existence of these quasi-ordered structures was first observed by Corrsin,[1] but it was Townsend[2] who emphasized the role played by these structures in the development of the turbulent flow. At present a large portion of experimental turbulence research is directed toward observation and isolation of these structures by flow visualization and conditional sampling techniques (Laufer[3] contains a review of the experimental research performed prior to 1975). In fact from laboratory observations in free turbulent shear flows,[4,5] it appears that the large-scale structure is a manifestation of mean inflectional velocity profile hydrodynamic instability and, as will be seen, it is this observation which motivates the description of the large-scale structure used here.

From the acoustician's standpoint, the experimental results concerning the role of these structures as sound generators have been somewhat contradictory. Crow[6] reported some experiments in subsonic jets suggesting that these structures were important as amplifiers of internal tones; however, Moore[7] produces results indicating that these structures do not radiate significant acoustic power themselves, but found, at high levels of jet excitation, an increase in radiated broadband noise.

The above indicates a need for continued research into the role the large-scale structures play in the sound generation process. The purpose of this study then is to examine the sound due to the large-scale (wavelike) structure in an infinite free turbulent shear layer. Specifically, this work is a computational study of a plane shear layer, which accounts, by way of a triple decomposition of the flowfield variables, for three distinct component scales of motion (mean, wave, turbulent), and from which the sound, due to the large-scale wave-like structures, in the acoustic field can be isolated by a simple phase average.

On the theoretical side, there have been varied attempts at computing noise from flowfields. For example, attempts at computing noise from discrete vortex models of flowfields have been made by Davies et al.[8] and Hardin and Mason,[9] who computed noise from a jet flow and from the flow over the mouth of a cavity, respectively. On the other hand, Ffowcs Williams and Kempton[10] modeled the large-scale structure of the jet as an instability wave that spatially grows and decays in amplitude. In addition, they also used a vortex

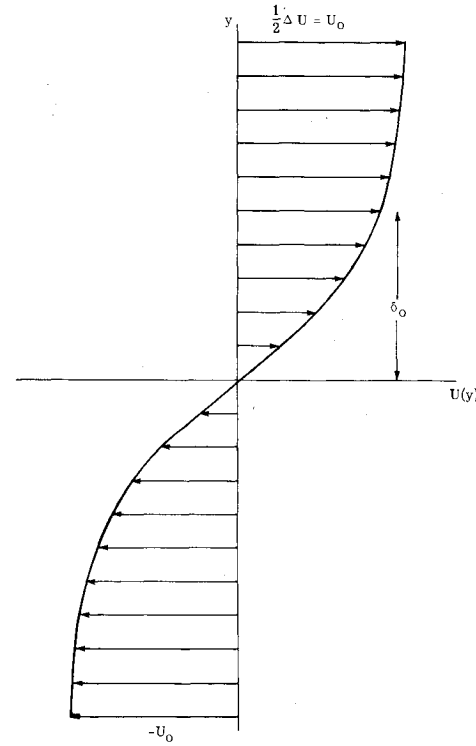

Fig. 1 Mean velocity profile.

Received Aug. 29, 1978; revision received Jan. 17, 1979. This paper is declared a work of the U.S. Government and therefore is in the public domain.

Index categories: Aeroacoustics; Viscous Nonboundary-Layer Flows.

*Research Scientist.

model to study the effect of coalescence on the sound generation process. Although the details of the flow and the dynamical processes involved differed, both Liu[11] and Morris[12] have examined the near-field noise produced by the large-scale wavelike structure in a jet using a triple decomposition technique to isolate the large-scale structure.

As mentioned previously, the goal here is to compute the sound caused by the wavelike structures in a free turbulent flow; however, in this study, Lighthill's theory is applied to the flowfield (source region) and, through the use of a phase average, the sound emitted, due to the large-scale structures, to the acoustic field is computed. The mathematical description of the flowfield in this work is governed by the results of Liu and Merkine,[13] who decomposed the flowfield variables of a plane turbulent shear layer into three components (mean, wave, and turbulent) and solved averaged energetic rate equations to determine the temporal evolution of both the large- and small-scale components. This temporal evolution is characterized by a growth and decay cycle for the wave energy. The mathematical description of the acoustic field is governed by Lighthill's theory and the appropriate solution integral of a convected wave equation for the pressure fluctuations. With the application of a phase average to the solution integral, the significant contribution to the pressure signal, due to the presence of the large-scale wavelike structure in the flow, is isolated. In addition, the effect of certain flow parameters on the level of sound produced is examined.

II. Mathematical Formulation of Flow Problem

Consider a free turbulent shear flow with the mean flow formed by the intersection of two horizontally parallel streams (see Fig. 1) flowing in opposite directions. The small-scale turbulence is assumed to have evolved to a self-preserving state and is in energetic equilibrium with the mean flow. At some instant ($t=0$), a large-scale instability wavelike structure is superimposed on this equilibrium field. Thus, at the initial time $t=0$, the flow is characterized by three distinct scales of motion (mean, wave, and turbulent). Since the mean flow and mean turbulent motions are independent of the horizontal x coordinate, the flow in the x direction is spatially periodic (with wavelength corresponding to that of the instability wave) and of infinite extent. The large-scale wavelike structure is taken as two-dimensional and spans the x-y (transverse direction) plane, and the small-scale turbulence is three-dimensional, but homogeneous in both the x and z (spanwise) directions. Figure 2 contains a sketch of the flow (source) field, with the distributions of mean velocity and mean Reynolds stress shown. Since the large- and small-scale motions are functions of time, the subsequent temporal evolution of these components is followed by solving the respective energetic rate equations. Gatski and Liu[14] have performed a computational study of this flow, but with the nonlinear evolution of the flow governed by differential rate equations for the various flow variables. In general, using this completely numerical approach to calculate the sound would be desirable, since in complicated flows a discrete distribution of flow variables is always computed and the techniques developed would be directly applicable. However, attempts to date to use this formulation have proved costly in terms of computer resources, thus making it necessary to consider, in this first attempt, the averaged energetic rate equation approach of Liu and Merkine[13] (hereafter denoted by LM). It should be noted that the LM approach does allow for the isolation of the large-scale structures in the sound calculations and, in comparison with the results of Ref. 14, reveal a similar behavior in the temporal evolution of the wave and turbulent energies (an important characteristic in the sound calculation), but a difference in the detailed transverse spatial distribution of the flow variables.

Since the flow formulation follows that of LM, only the essential features will be presented here; for further details the reader is referred to Ref. 13. In addition, throughout the paper all quantities are made dimensionless by the half-velocity difference $\frac{1}{2}\Delta U = U_0$ and an initial shear layer thickness δ_0 (defined as the variance of the velocity gradient distribution, $[\int y^2 U_y \mathrm{d}y / \int U_y \mathrm{d}y]^{1/2}$. The averaged kinetic energy equation for the large structure can be written as

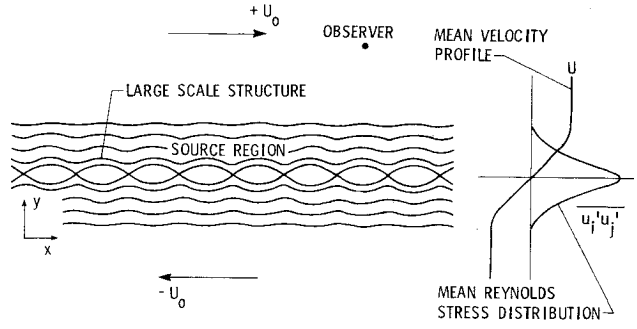

Fig. 2 Sketch of source and acoustic fields.

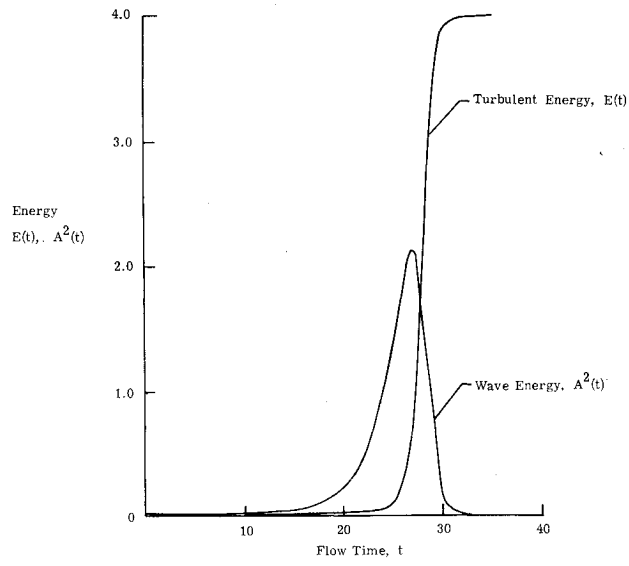

Fig. 3 Temporal evolution of wave and turbulent energies.

$$\frac{1}{2}\frac{\mathrm{d}}{\mathrm{d}t}\int_{-\infty}^{\infty}\overline{(\tilde{u}^2+\tilde{v}^2)}\,\mathrm{d}y=\int_{-\infty}^{\infty}-\overline{\tilde{u}\tilde{v}}\frac{\partial U}{\partial y}\,\mathrm{d}y-\int_{-\infty}^{\infty}-\left[\overline{\tilde{r}^{11}\frac{\partial\tilde{u}}{\partial x}+\tilde{r}^{12}\left(\frac{\partial\tilde{u}}{\partial y}+\frac{\partial\tilde{v}}{\partial x}\right)+\tilde{r}^{22}\frac{\partial\tilde{v}}{\partial y}}\right]\mathrm{d}y \tag{1}$$

with

$$\tilde{r}^{11}=\langle u'^2\rangle-\overline{u'^2},\quad \tilde{r}^{22}=\langle v'^2\rangle-\overline{v'^2},\quad \tilde{r}^{12}=\langle u'v'\rangle-\overline{u'v'} \tag{2}$$

where $\tilde{u}(x,y,t)$, $\tilde{v}(x,y,t)$ are the dimensionless horizontal (x-component) and vertical (y-component) large-scale velocities, $U(y)$ is the dimensionless mean flow horizontal velocity, $\tilde{r}^{ij}(x,y,t)$ is the wave-induced stress tensor, and $u'(x,y,z,t)$, $v'(x,y,z,t)$ are the dimensionless x and y small-scale turbulent velocity components, respectively. The angular brackets denote a phase average and the overbar denotes a horizontal average over at least one wavelength of the large-scale wavelike structure. It should be noted that in Eq. (1) we have taken the integrated viscous dissipation to be small. Equation (1) simply states that the change of large-scale energy is due to that *interchanged* between the mean flow and large-scale structure and the energy *lost* to the small-scale

turbulence.[14] Next, consider the averaged small-scale turbulent kinetic energy equation

$$\frac{1}{2}\frac{\mathrm{d}}{\mathrm{d}t}\int_{-\infty}^{\infty}\overline{(u'^2+v'^2+w'^2)}=\int_{-\infty}^{\infty}-\overline{u'v'}\frac{\partial U}{\partial y}\,\mathrm{d}y+\int_{-\infty}^{\infty}$$

$$-\left[\overline{\tilde{r}^{11}\frac{\partial\tilde{u}}{\partial x}+\tilde{r}^{12}\left(\frac{\partial\tilde{u}}{\partial y}+\frac{\partial\tilde{v}}{\partial x}\right)+\tilde{r}^{22}\frac{\partial\tilde{v}}{\partial y}}\right]\mathrm{d}y-\epsilon \tag{3}$$

where ϵ is the averaged integrated viscous dissipation. Since the turbulence is three-dimensional, Eq. (3) contains the spanwise (z-component) velocity w'. The rate of change of the averaged turbulent kinetic energy results from a *gain* of energy by the action of the mean Reynolds stresses on the mean velocity gradient, a *gain* of energy due to the interaction of the wave-induced stresses and wave velocity gradients, and a loss of energy by the action of small-scale viscous dissipation. As can be seen from the above energy equations, a great many closure problems, such as those involving the pressure-strain correlation, have been eliminated by the integral formulation that has been used. The remaining unknown terms are handled by means of various shape assumptions.

Continuing with the development of LM, one can immediately write the shape assumptions for the mean velocity and mean Reynolds stresses. Since for the purpose of this study it is sufficient to consider the parallel flow case, the mean velocity profile can be written as

$$U=\tanh y \tag{4}$$

and the mean Reynolds stress can be written as

$$\begin{bmatrix}\overline{u'^2}\\ \overline{v'^2}\\ \overline{w'^2}\\ -\overline{u'v'}\end{bmatrix}=\frac{2E(t)}{3\sqrt{\pi}}\begin{bmatrix}1+2\beta\\ 1-\beta\\ 1-\beta\\ \dfrac{1-\beta}{c_T}\end{bmatrix}e^{-y^2} \tag{5}$$

where β represents the ratio of the time scale for return to isotropy to that of dissipation and c_T represents the ratio of the rate of strain time scale to that of return to isotropy. From the results of Lumley[15] for the homogeneous shear problem, the constant coefficients β and c_T are equal to 0.242 and 1.445, respectively. The functional form of the vertical distribution is assumed from the results of Wygnanski and Fiedler[16] for a two-dimensional mixing region. Finally, the time history of the evolution of the total turbulent kinetic energy is contained in the function $E(t)$. The most important aspect of this shape assumption for the mean Reynolds stress tensor is the fact that this is an equilibrium form, giving a balance (in the absence of the wave) between mean flow energy production and viscous dissipation. In addition, the above spatial distributions are representative of self-preserving distributions, and such an energetic equilibrium, in terms of self-preserving variables, can be achieved from a solution of differential rate equations for this flow.[14] Thus, any subsequent evolution of the energy as described by $E(t)$ is due solely to the integrated interaction between the wave-induced stresses and the disturbance velocity gradients. It should be noted that if the flow were inhomogeneous in the streamwise direction, it would be necessary to account for this flow divergence through a mean flow rate equation. In addition, since the shear layer thickness would be increasing, the (local) wavenumber and frequency would become a function of position.[17] The formulation presented here is most appropriate for regions of the flow where a locally parallel flow assumption can be made. Next, the shape functions for the large-scale wavelike structures are established.

The spatial distributions for the wave are taken from linear theory, while the temporal evolution is governed by an amplitude function $A(t)$, which is solved for simultaneously with the turbulent function $E(t)$. The disturbance velocities are written as

$$\begin{bmatrix}\tilde{u}(x,y,t)\\ \tilde{v}(x,y,t)\end{bmatrix}=A(t)\begin{bmatrix}\Phi_y(y;\alpha)\\ i\alpha\Phi(y;\alpha)\end{bmatrix}\exp(i\alpha x)+\text{c.c.} \tag{6}$$

where Φ is the disturbance eigenfunction, α is the local wavenumber and c.c. denotes the complex conjugate of the first term on the right-hand side. The structure of the wave-induced stresses can be inferred from the shape functions for the wave velocities and mean Reynolds stresses. Since the wave-induced stresses are essentially perturbations, caused by the presence of the wave, of the mean Reynolds stresses, it is consistent to write the shape functions for the wave-induced stresses as

$$\tilde{r}^{ij}=A(t)E(t)r^{ij}(y;\alpha)\exp(i\alpha x)+\text{c.c.} \tag{7}$$

As was shown in LM, the eigenfunctions satisfy the Rayleigh equation, to lowest order, and the wave-induced stresses satisfy the linearized transport equations[18]

$$i\alpha(U-c)\begin{bmatrix}r^{11}\\ r^{22}\\ r^{33}\\ r^{12}\end{bmatrix}+\underbrace{\begin{bmatrix}2r^{12}\\ 0\\ 0\\ r^{22}\end{bmatrix}}_{\text{production}}U_y+\frac{1}{T}\underbrace{\begin{bmatrix}r^{11}\\ r^{22}\\ r^{33}\\ r^{12}\end{bmatrix}}_{\text{advection by mean flow}}-\frac{1}{3}\underbrace{\begin{bmatrix}r^{ii}\\ r^{ii}\\ r^{ii}\\ 0\end{bmatrix}}_{\text{pressure-strain correlation}}$$

$$+\frac{\beta}{3T}\underbrace{\begin{bmatrix}r^{ii}\\ r^{ii}\\ r^{ii}\\ 0\end{bmatrix}}_{\text{dissipation}}=i\alpha\phi\underbrace{\begin{bmatrix}\overline{u'^2}\\ \overline{v'^2}\\ \overline{w'^2}\\ -\overline{u'v'}\end{bmatrix}}_{\substack{\text{vertical advection}\\ \text{of mean stress by wave}}}$$

$$+\underbrace{\begin{bmatrix}-2\overline{u'^2}i\alpha\phi_y+2\overline{u'v'}\phi_{yy}\\ 2\overline{v'^2}i\alpha\phi_y+2\overline{u'v'}\alpha^2\phi\\ 0\\ -\overline{v'^2}\phi_{yy}-\overline{u'^2}\alpha^2\phi\end{bmatrix}}_{\substack{\text{work done by mean stress}\\ \text{against wave strain rates}}} \tag{8}$$

where c is the wave velocity (in this temporal instability problem c is pure imaginary), U_y is the mean velocity gradient, T is the time scale for return to isotropy, and the ϕ are solutions to the Rayleigh equation (i.e., $\Phi\simeq\phi$ to lowest order). Note that the pressure-strain correlation has been modeled following Rotta[19] (see also Lumley[15]), and the dissipation has been assumed proportional to the trace of the wave-induced stress tensor matrix with no variation of the time scale T allowed. Finally, there is one further simplification that can be made at this point. Since the mean flow does not change in this problem, the production of small-scale turbulent energy in Eq. (3) is only altered through the time history of the turbulent energy $E(t)$. In addition, as was seen in the closure of the equations for the wave-induced stresses, the time scale for return to isotropy was not altered by the presence of the wave and the viscous dissipation of the large-scale wave was neglected. In light of the time scale similarity between return to isotropy and dissipation ($\beta=\text{const.}$[15]), an

unperturbed time scale for return to isotropy means an unperturbed time scale for dissipation; thus, implying that the small-scale energy dissipation is in quasiequilibrium with the small-scale energy production throughout the temporal evolution of the wave energy. It should be emphasized that this approximate balance between small-scale turbulent energy production and dissipation is an artifact of the parallel flow assumption and the equilibrium spatial distribution assumed for the shape functions of the mean Reynolds stresses, Eq. (5). In the absence of such assumptions, as was the case in Gatski and Liu,[14] the expected result that both small-scale energy production and dissipation varied as a function of time was obtained.

An examination of Eqs. (1-8) shows that the spatial distributions of all variables have either been assumed [Eqs. (4) and (5) for the mean velocity and mean Reynolds stresses] or can be obtained through the numerical solution of ordinary differential equations (the Rayleigh equation for the eigenfunctions and the transport equations for the wave-induced stresses). With this information, the averaged energetic rate equations for the large-scale energy, Eq. (1), and the small-scale energy, Eq. (3), reduce to the following equations for $A^2(t)$ and $E(t)$ (Ref. 13)

$$\frac{dA^2}{dt} = A^2 \tilde{I}_{rs} - A^2 E I_{wt} \tag{9a}$$

$$\frac{dE}{dt} = A^2 E I_{wt} \tag{9b}$$

where

$$\tilde{I}_{rs}(\alpha) = i\alpha \int_{-\infty}^{\infty} (\phi \phi_y^* - \phi^* \phi_y) \operatorname{sech}^2 y \, dy \tag{10}$$

$$I_{wt}(\alpha) = \int_{-\infty}^{\infty} -r^{11}(-i\alpha\phi_y^*) + r^{11*}(i\alpha\phi_y) + r^{12}(\phi_{yy}^* + \alpha^2\phi^*)$$
$$+ r^{12*}(\phi_{yy} + \alpha^2\phi) + r^{22}(i\alpha\phi_y^*) + r^{22*}(-i\alpha\phi_y)\, dy \tag{11}$$

(the asterisk denotes complex conjugate); with initial conditions at $t=0$: $A^2 = A_0^2$ and $E = E_0$. For the most amplified disturbance of the hyperbolic tangent profile, $\alpha = 0.4446$ (Ref. 20), the interaction integrals $\tilde{I}_{rs}$ and I_{wt} are equal to 0.3804 and 0.5760, respectively. Of course, in the numerical evaluation of the integrals, the limits of integration are finite and are taken to be sufficiently large to include all significant contributions. The value for $\tilde{I}_{rs}$ is quite close to that obtained by LM; however, the value for I_{wt} is slightly different. The exact reason for the discrepancy is unknown, but may be attributed to too coarse a mesh in the integration of the interaction integral; however, a check on the results in Sec. IV using the LM value of I_{wt} produced no qualitative change in the wave and turbulent kinetic energy profiles. It should be noted that the vector diagrams for the eigenfunctions ϕ (recall $\Phi \simeq \phi$) and their derivatives and the wave-induced stresses were found to correspond to those obtained by LM.

Unless otherwise noted, the values $A_0^2 = 10^{-4}$ and $E_0 = 10^{-2}$ were taken for the initial wave and turbulent energies, respectively, throughout this study. This corresponds to a rather weak perturbation energy relative to the small-scale turbulent energy. The specification of the initial conditions allows the set of equations in Eq. (9) to be solved (by fourth order Runge-Kutta). In Fig. 3, the resulting temporal behavior of the solution functions $A^2(t)$, wave energy, and $E(t)$, small-scale turbulent energy, are shown (cf. Ref. 14). As can be seen [refer to Eqs. (9)], the initial rate of change of wave energy is positive, thus causing both the wave and small-scale energies to grow; however, at some time, the energy drain from the large- to the small-scale balances, and then exceeds, the production of large-scale energy, thus causing the subsequent decay of the large-scale energy and the stabilizing of the small-scale energy at a new higher equilibrium level.

Finally, an examination of Eqs. (4-7) for the mean and wave velocities and stresses reveals that both their temporal and spatial behavior is now known. With this information the flowfield is sufficiently determined to utilize Lighthill's theory and compute the noise from this source field.

Mathematical Formulation of Acoustic Problem

The source region is the flow domain and outside of the source region, in the acoustic field, the observer is in a region of nonzero uniform velocity (Fig. 2). In addition, since the Lighthill acoustic analogy is being applied to the flowfield, it is unnecessary to take into account any effect of the nonuniform mean velocity on the sound propagation within the source region. However, since the source propagates through a uniformly moving medium, it is necessary to write a convective form of the wave equation for the density fluctuations,[21]

$$\frac{D^2\rho}{D\tilde{t}^2} - \frac{1}{M^2}\frac{\partial^2\rho}{\partial x_i \partial x_i} = \frac{\partial^2 T_{ij}}{\partial x_i \partial x_j} \tag{12}$$

where

$$\frac{D}{D\tilde{t}} = \frac{\partial}{\partial \tilde{t}} + U_\infty \frac{\partial}{\partial x}, \quad (U_\infty = 1)$$

$M(=U_0/a_0$, a_0 is the ambient speed of sound) is the freestream Mach number, T_{ij} is the Lighthill stress tensor, and, as before, all the variables have been made dimensionless by the half-velocity difference, shear layer thickness, and ambient density ρ_0. The usual general form of T_{ij} can be simplified by noting that the flow here is subsonic and isotropic, that viscous effects have been neglected relative to the Reynolds stresses, and that density fluctuations are assumed negligible within the source region. With these assumptions, one can write for the dimensionless stress tensor

$$T_{ij} \simeq u_i u_j \tag{13}$$

where the velocities are referenced relative to coordinate axes moving with the freestream velocity U_∞. Since Crow's[22] analysis showed that, to lowest order, u_i is the solenoidal velocity, it can be decomposed into its three component velocities and written as

$$u_i = \underset{\text{mean}}{(U - U_\infty)\delta_{i1}} + \underset{\text{wave}}{\tilde{u}_i} + \underset{\substack{\text{small-scale}\\ \text{turbulence}}}{u_i'} \tag{14}$$

where, after applying a phase average,

$$\langle u_i \rangle = (U - U_\infty)\delta_{i1} + \tilde{u}_i \tag{15}$$

The solution to the inhomogeneous convective wave equation (12) can be written in terms of the pressure fluctuations as[23]:

$$p(\zeta_i, \tilde{t}) = \frac{1}{4\pi} \iiint_{\text{vol}} \frac{1}{r} T_{ij,ji}(x,y,t)\, dz\, dy\, dx \tag{16}$$

where

$$t = \tilde{t} + [M(\zeta_1 - x) - r]M/\beta_M^2$$

$$r = \{(\zeta_1 - x)^2 + \beta_M^2[(\zeta_2 - y)^2 + (\zeta_3 - z)^2]\}^{1/2}$$

$$\beta_M^2 = 1 - M^2$$

ζ_i are the coordinates of the observer in the acoustic field, and, as can be seen, no far-field approximations have been

made. It is necessary at this point to elaborate on the volume integration needed in Eq. (16). Even though homogeneity was assumed in the z direction ($\partial/\partial z = 0$) in the flow problem, the variables t and r are both functions of z; thus making it desirable to include an integration of unit length ($z = -0.5$ to $z = 0.5$) in the z direction. Other workers[24-26] have also accounted for this direction, even though their essential flow dynamics have also been in a plane perpendicular to this direction. For example, Michalke,[24] who used a two-dimensional linear instability wave model for the disturbance flow, was able to obtain a known analytic function (Hankel function) using infinite limits of integration in the z direction. Powell,[25] who used a vortex model, computed solutions per unit length in the z direction, and Hardin,[26] who also used a vortex model, assumed an effective length in the z direction. The remaining integrations in the y and x directions are fixed by the dynamics of the flow itself. In the y direction, the limits of integration are set at the points where the eigenfunctions ϕ and ϕ_y are at least an order of magnitude smaller than the values at the center of the shear layer. This region then includes a large portion of the flowfield where the variation of mean flow velocity is zero and the disturbance energetics are negligible. In the x direction, the size of the integration region was fixed after the retarded times, determined by varying the x bounds of the regions, were less than the initial time ($t = 0$) when the large-scale wave was superimposed on the equilibrium turbulent flow.

As mentioned in previous sections, the interest in this work is in the sound caused by the large-scale structures. This contribution to the pressure fluctuations in the acoustic field can be determined by applying a phase average to Eq. (16),

$$\tilde{p}(\zeta_i,\tilde{t}) = \frac{1}{4\pi}\int\int\int_{\text{vol}} \frac{1}{r}\langle T_{ij,ji}\rangle \,\mathrm{d}z\mathrm{d}y\mathrm{d}x \tag{17}$$

where

$$\langle T_{ij,ji}\rangle = \langle T_{11,11}\rangle + 2\langle T_{12,21}\rangle + \langle T_{22,22}\rangle = 2[(\tilde{u}_x)^2 + (U_y+\tilde{u}_y)\tilde{v}_x] + \tilde{r}^{11}_{xx} + 2\tilde{r}^{12}_{xy} + \tilde{r}^{22}_{yy} + (\overline{v'^2})_{yy}$$

and the integrand is evaluated at a retarded time. The above expression for the stress tensor is composed of the usual self and shear noise terms; in addition, there are gradients of the wave-induced and mean (spatial) Reynolds stresses present. These stress tensor gradients are due to the presence of the wave and the application of the phase average. If the shape functions are substituted into Eq. (17), the resulting component expression for the pressure fluctuations is

$$\tilde{p} = \tilde{p}_{\text{SN}} + \tilde{p}_{\text{SHN}} + \tilde{p}_{\text{WISG}} + \tilde{p}_{\text{MTSG}} \tag{18}$$

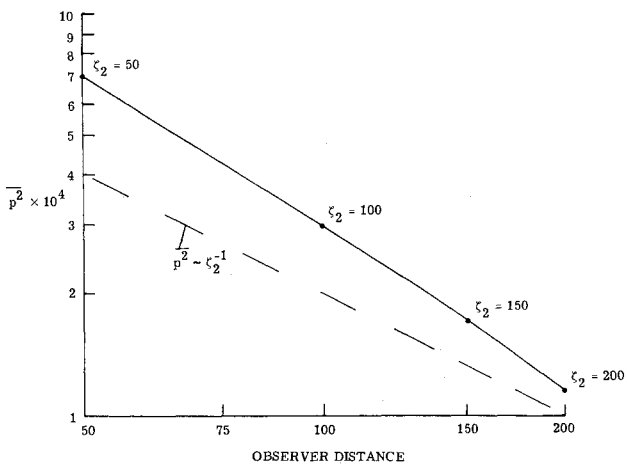

Fig. 4 Spatial variation of mean square pressure.

with self noise:

$$\tilde{p}_{\text{SN}}(\zeta_i,\tilde{t}) = \frac{\alpha^2}{\pi}\int\int\int_{xyz}\int\Big\{|2\,|\phi_y|^2\sin^2(\alpha x+\theta') + |\phi|\,|\phi_{yy}|\,[\cos(2\alpha x+\theta+\theta'')]\Big\}\frac{A^2(t)}{r}\,\mathrm{d}z\mathrm{d}y\mathrm{d}x \tag{19}$$

shear noise:

$$\tilde{p}_{\text{SHN}}(\zeta_i,\tilde{t}) = \frac{\alpha^2}{\pi}\int\int\int_{xyz}|\phi|\,\mathrm{sech}^2 y\cos(\alpha x+\theta)\frac{A(t)}{r}\,\mathrm{d}z\mathrm{d}y\mathrm{d}x \tag{20}$$

wave-induced stress gradients:

$$\tilde{p}_{\text{WISG}}(\zeta_i,t) = \frac{1}{2\pi}\int\int\int_{xyz}\int\Big\{-\alpha^2\,|r^{11}|\cos(\alpha x+\theta^{11}) + r^{12}_{xy} + r^{22}_{yy}\Big\}\frac{A(t)E(t)}{r}\mathrm{d}z\mathrm{d}y\mathrm{d}x \tag{21}$$

mean turbulent stress gradient:

$$\tilde{p}_{\text{MTSG}}(\zeta_i,\tilde{t}) = \frac{(1-\beta)}{3\pi^{3/2}}\int\int\int_{xyz}(2y^2-1)e^{-y^2}\frac{E(t)}{r}\,\mathrm{d}z\mathrm{d}y\mathrm{d}x \tag{22}$$

where

$$\phi = |\phi|e^{i\theta},\quad \phi_y = |\phi_y|e^{i\theta'},\quad \phi_{yy} = |\phi_{yy}|e^{i\theta''}$$

$$r^{11} = |r^{11}|e^{i\theta^{11}},\quad r^{12} = |r^{12}|e^{i\theta^{12}},\quad r^{22} = |r^{22}|e^{i\theta^{22}}$$

and the phase angles are functions of y. Recall that the vertical (y) distribution of the eigenfunctions and wave-induced stresses were numerically computed from the Rayleigh equation and Eq. (8), respectively. This requires finite-difference approximations for all y derivatives; for example, from Eq. (21)

$$r^{12}_{xy} = -\frac{\alpha}{\Delta y}\left[\,|r^{12}|_{j+1}\sin(\alpha x+[\theta^{12}]_{j+1}) - |r^{12}|_{j-1}\sin(\alpha x+[\theta^{12}]_{j-1})\right] + O(\Delta y^2) \tag{23}$$

$$r^{22}_{yy} = (\Delta y)^{-2}\left[\,|r^{22}|_{j+1}\cos(\alpha x+[\theta^{22}]_{j+1}) - 2\,|r^{22}|_j\cos(\alpha x+[\theta^{22}]_j) + |r^{22}|_{j-1}\cos(\alpha x+[\theta^{22}]_{j-1})\right] + O(\Delta y^2) \tag{24}$$

where Δy is the spacing between grid points and the difference approximations are taken about the grid point j. Since the discrete distribution of the integrands is known as a function of both space and time, the integrals in Eqs. (19-22) can be evaluated. It is interesting in the present formulation to note that, in the absence of the wave (either for $t < 0$ or at the end of the decay cycle $t \gtrsim 35$, see Fig. 3), the only contribution to $\tilde{p}$ is from the mean turbulence stress gradient, Eq. (22). However, in the absence of the wave, the small-scale turbulence and mean flow are in energetic equilibrium thus making the rate of change of mean small-scale energy a constant and therefore producing no sound in the acoustic far field. Now that the theoretical development is complete, the pressure fluctuations in the acoustic field can be computed.

IV. Results

As mentioned in the previous section, no far-field approximations have been made in the solution integral of Eq.

(17). However, as it is the goal here to examine the acoustic far field, it is necessary to examine the mean square acoustic pressure for its variation with distance from the source region. For a point source, the far-field variation of the mean square pressure is the inverse square law; however, in this problem the source is dominated by the two-dimensional dynamics of the flow. The spanwise z coordinate here plays a role similar to that played in the Michalke[24] problem as far as spatial variation of mean square pressure in the far field is concerned. In the Michalke work, the instability had the usual exponential traveling wave form from which, upon integration in the z direction (with infinite limits of integration) yielded a Hankel function distribution in the x and y directions. In this work, the functional form of the instability is unknown and the acoustic far-field behavior must be computed, although the Michalke result can certainly serve as a guide as far as any far-field mean square pressure decay is concerned. The variation of p^2 with distance from the shear layer is shown in Fig. 4. Note that the decay with distance is quicker than ζ_2^{-1} (note, this is mean *square* pressure), but considering the limits of integration, which are finite and dependent on the temporal length of the growth and decay cycle of the wave energy, the trend is evident and consistent[24] with an essentially two-dimensional flowfield.

Consider the sound signal at the observer point ($\zeta_1 = 0$, $\zeta_2 = 200$, $\zeta_3 = 0$), which, from the results of Fig. 4, is taken here to be in the acoustic far field. (Note that in the remainder of this paper all observer locations will be fixed by the ζ_2 coordinate, since all the results presented are in the ζ_1-ζ_2 plane, $\zeta_3 = 0$, and at the same origin point $\zeta_1 = 0$.) In Fig. 5, the computed acoustic pressure fluctuations are plotted as a function of time. This "signal" was formed by computing a pressure value every $\Delta\tilde{t} = 1.25$. This sampling frequency results from the fact that the Strouhal number ($\equiv f\delta_0/U_0$) of acoustic far-field pressure fluctuations produced by the large-scale structure is $\alpha/2\pi M$. In this problem, the Mach number ($= U_0/a_0$) of the flow is 0.3 and the wave number (dimensionless) of the most amplified disturbance (for the hyperbolic tangent velocity profile) is 0.4446; thus giving a Strouhal number of 0.24. The value of $\Delta\tilde{t}$ used is less than the corresponding calculated period and is a compromise between resolution and computational time. It should be noted that the pressure signal does not reach the observer at $\zeta_2 = 200$ until an elapsed time of $\tilde{t} = 60$ (where $t = 0$ corresponds to the beginning of wave growth). This is due to the sonic propagation velocity from the source region where, in dimensionless variables, $\tilde{t} = M\zeta_2$. The length of the source record used was 200 (from $\tilde{t} = 60$ to $\tilde{t} = 260$) and was determined by the number of samples necessary to get a relatively stationary value for p^2 (note that all the results presented here were based on pressure signals of temporal length 200).

It is instructive at this point to compare the time history of the wave and turbulent energies (Fig. 3) with the time history of the pressure fluctuations at the observer point $\zeta_2 = 200$ (Fig. 5), since all flow time history effects are contained in the functions $A(t)$ and $E(t)$ [see Eqs. (19-22)]. The most striking difference between Figs. 3 and 5 is the apparent abundance of frequencies present in the pressure signal. This is due to the fact that the inclusion of retarded time effects causes *different regions* of the source (flow) to contribute, at *different flow times*, to the pressure fluctuation $\tilde{p}$ at a *fixed observer time*. For example, at large enough observer times, when the entire time history of the source (flow), $0 < t \lesssim 35$, is included in the computation of a fluctuating pressure value at a *fixed observer time*, the source (flow) region contributing at flow times of t_1 to t_2 is *out of phase* with the source (flow) region contributing at flow times of t_3 to t_4. It is important to emphasize that, because of the differing contributions to the total fluctuating pressure signal from different source (flow) regions, it is essential that the source region be large enough so as to include all flow time effects back to $t = 0$ (recall that for $t < 0$, and also for $t \gtrsim 35$, no sound was produced). This source region size directly applies to the horizontal x coordinate (making it nonarbitrary and dependent on the flow dynamics), since, as was stated earlier, the y coordinate limits are fixed by the flow dynamics and the z coordinate limits are arbitrary, but predetermined. It will become apparent later which ranges of flow times are important in the sound production process.

The spectrum of the computed pressure signal at $\zeta_2 = 200$ is shown in Fig. 6. The figure shows that the spectrum is narrow-band with the peak occurring at a Strouhal number of 0.175. It should be noted that the calculated Strouhal number of 0.24 did not account for any Doppler effect which, of course, does occur here, since the sound is propagating in a uniformly moving medium. The absence of any broadband noise in the spectrum is an artifact of the isolation of the large-scale structure effects by the phase average. In the flow formulation used here,[13] the spatial size and shape of the large-scale wave does not change, but the amplitude of the structure does change, as a function of time; thus, possibly also precluding the existence of broadband noise sources. There are other local maxima in the pressure spectrum shown. Since these maxima are smeared somewhat at this large observer distance, it is instructive to look at the pressure spectrum at shorter observer distances (see Figs. 7a, b, c). As is seen for $\zeta_2 = 50$, Fig. 7a, the harmonic (with respect to the wavelength of the initial instability wave) spikes are quite

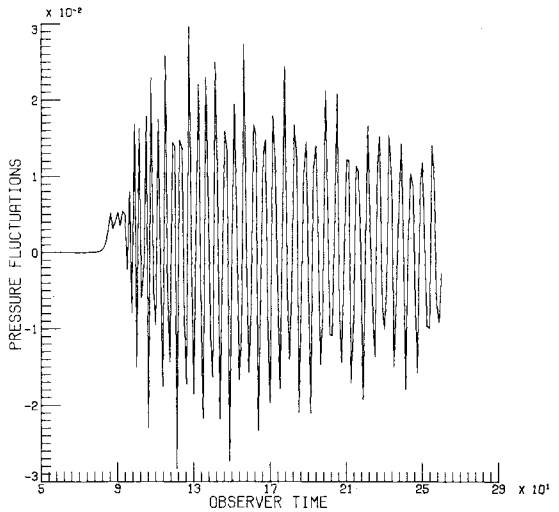

Fig. 5 Pressure signal at $\zeta_2 = 200$ for $A_0^2 = 10^{-4}$, $E_0 = 10^{-2}$.

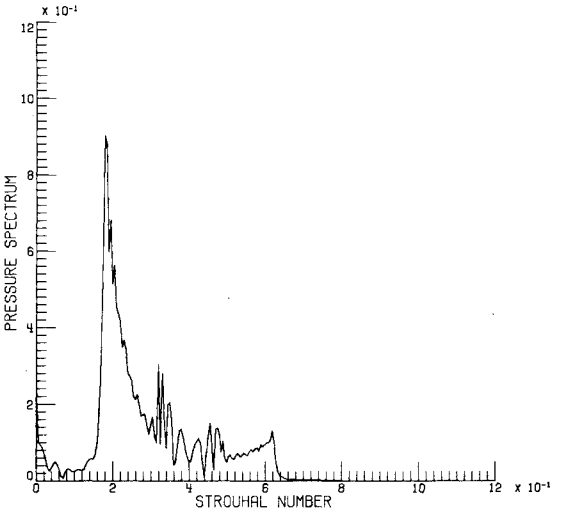

Fig. 6 Pressure spectrum at $\zeta_2 = 200$ for $A_0^2 = 10^{-4}$, $E_0 = 10^{-2}$.

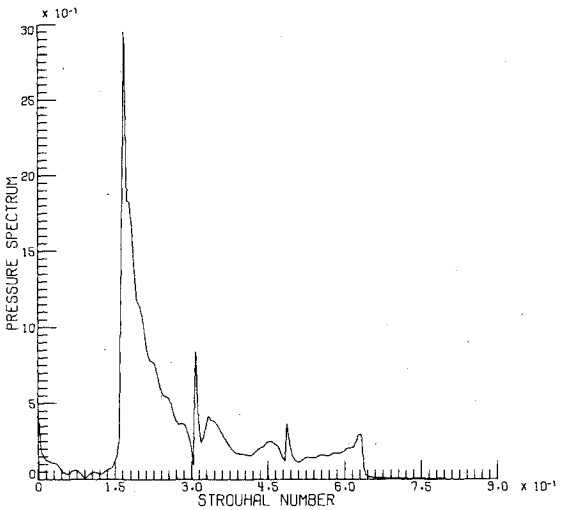

Fig. 7a Pressure spectrum at $\zeta_2 = 50$.

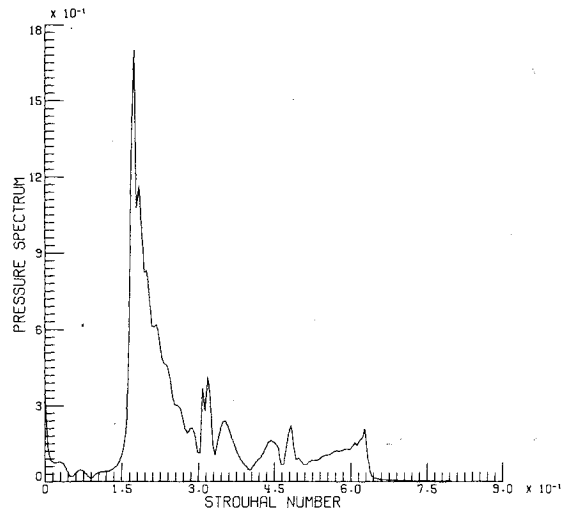

Fig. 7b Pressure spectrum at $\zeta_2 = 100$.

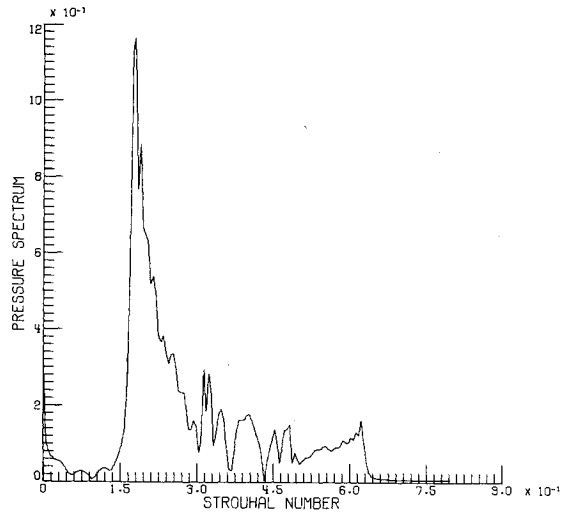

Fig. 7c Pressure spectrum at $\zeta_2 = 150$.

distinct; however, as the observer distance increases (Figs. 7b, 7c) other local maxima begin to appear and the harmonic features are lost.

One of the more pertinent questions to ask at this point is which of the four components of the total pressure signal,

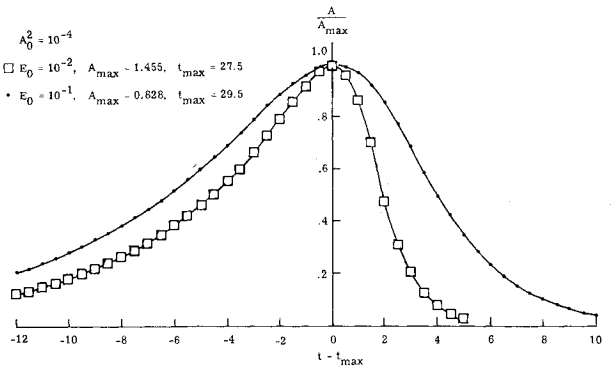

Fig. 8 Normalized growth and decay cycle of wave amplitudes.

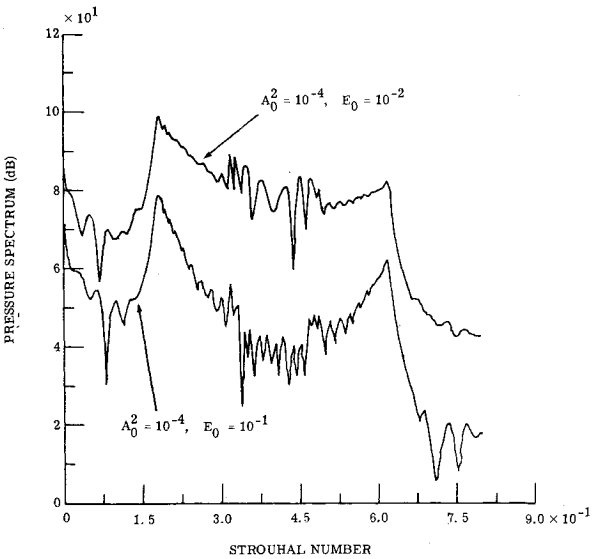

Fig. 9 Pressure spectrum at $\zeta_2 = 200$ for $A_0^2 = 10^{-4}$, $E_0 = 10^{-2}$ and $A_0^2 = 10^{-4}$, $E_0 = 10^{-1}$.

discussed in the previous section, contributes significantly to the acoustic radiation. This question can be easily answered in light of the formulation used in this work. For example, each contribution to the pressure signal—the self-noise, the shear noise, the wave-induced stress gradients, and the mean turbulent stress gradient, Eqs. (19-22)—can be isolated and its contribution determined. Such an analysis showed that the wave-induced stress gradients were the most significant contributors to the total pressure signal. This indicates that the overall sound produced is not a manifestation of only the large or small scales but rather a by-product of the interaction of the two scales as represented by the wave-induced stresses. This finding also sheds additional light on the experimental results of Moore,[7] who found that all the extra broadband noise comes from the area where the wave breaks. Ffowcs Williams and Kempton[10] suggest that this indicates that "it is the large-scale structure itself, and not an increase in background turbulence, which makes the extra broadband noise." Even though there is no phase randomness (as in Ffowcs Williams and Kempton) explicitly included in this model, the above result indicating the importance of the wave-induced stresses also supports Moore's result, since an increase in wave amplitude (additional forcing) would increase the wave-induced perturbations on the small-scale (random) turbulent stress field. This would have a dispersing effect on the sound field, thus generating more broad-band noise. It should be pointed out that the parallel flow assumption has precluded any change in the mean velocity distribution. In a real flow, the shear noise terms would be affected through a change in the spatial distribution of the

mean velocity. However, in such a diverging flow, as the shear layer thickens (increasing source region size) the value of maximum mean shear decreases, thus making it unclear how these two effects would alter (if at all) the contribution of the shear noise term.

Another result obtained here for a wave with no phase randomness, but consistent with the results of Ffowcs Williams and Kempton,[10] is that the sound decreases for a decrease in large-scale disturbance amplitude and a decrease in the rate of change of disturbance amplitude at the "break-point" where transition from growth to decay occurs (even though the disturbance in Ref. 10 varied spatially, an analogy can be made here). To show this effect, let the initial turbulent energy E_0 be changed to 10^{-1}. This causes the maximum wave energy, $A^2_{\max}$, to decrease to 0.6855 (from $A^2_{\max} = 2.116$ for the case $E_0 = 10^{-2}$, $A^2_0 = 10^{-4}$) and for the temporal location of the break-point, $t_{\max}$, to shift to 29.5 (from $t_{\max} = 27.5$ for the case $E_0 = 10^{-2}$, $A^2_0 = 10^{-4}$). A comparison of the two cases is shown in Fig. 8, with the wave amplitudes normalized by the respective $A_{\max}$ and the time axis origin centered about the respective $t_{\max}$. Two changes have occurred in the wave amplitude temporal distribution by changing the initial small-scale turbulent energy from $E_0 = 10^{-2}$ to $E_0 = 10^{-1}$ (with $A^2_0 = 10^{-4}$): The first is that the maximum wave amplitude $A_{\max}$ at the break-point $t_{\max}$ has decreased 43% and the second is that the rate of change of wave disturbance amplitude has decreased. This means that the sound produced should be less than that computed for $\zeta_2 = 200$ earlier (see Fig. 6). In Fig. 9, a comparison of the two pressure spectra (with arbitrary normalization) is shown, which indeed shows a decrease in the amplitude ($\simeq 20$ dB) of the spectrum at the peak frequency consistent with the results of Ref. 10. It should be noted that this reduction in peak spectral amplitude is not due solely to the reduction in wave amplitude. Recall that the chief contributor to the pressure signal was the wave-induced stress gradients. As can be seen from Eq. (21), the time history effects are represented by the product of both the wave and turbulent energies. As a point of comparison, consider this product at $t_{\max}$ (see Fig. 8) for both cases of interest, that is, for the cases $A^2_0 = 10^{-4}$, $E_0 = 10^{-2}$, and $A^2_0 = 10^{-4}$, and $E_0 = 10^{-1}$. For the case $E_0 = 10^{-2}$, the product $A(t_{\max})E(t_{\max})$ is equal to 0.92, and for the case $E_0 = 10^{-1}$, the product equals 0.52. The reduction in $A(t_{\max})E(t_{\max})$ is less than a factor of 2, whereas the reduction in peak spectral amplitude is a factor of 10. This, of course, implies that the time scale over which the amplitude of the disturbance changes significantly is also a factor in the amount the sound is reduced.

This work has provided a means of bringing some of the difficulties of computing noise directly from a discrete distribution of flow variables, obtained from conservation and transport equations, into better focus as well as to shed additional light on the connection between the sound produced and the flow mechanisms responsible. Even though in more complicated flows the representation of the large-scale structure is not as straightforward as used here and more sophisticated averaging techniques and representations of the flow may be required, the overall approach taken in this study appears to be applicable in computing the sound due to large-scale coherent structures in turbulent flowfields.

Acknowledgment

The author wishes to thank J. C. Hardin for his helpful comments during the course of the investigation.

References

[1] Corrsin, S., "Investigation of Flow in an Axially Symmetric Heated Jet of Air," NACA Adv. Conf. Rept. No. 3123 (also W-94), 1943.

[2] Townsend, A. A., *The Structure of Turbulent Shear Flow*, 1st ed., Cambridge University Press, New York, 1956, Chap. 5.

[3] Laufer, J., "New Trends in Experimental Turbulence Research," *Annual Review of Fluid Mechanics*, Vol. 7, Annual Reviews, Inc., Palo Alto, Calif., 1975, pp. 307-326.

[4] Brown, G. L. and Roshko, A., "On Density Effects and Large Structure in Turbulent Mixing Layer," *Journal of Fluid Mechanics*, Vol. 64, Pt. 4, 1974, pp. 775-816.

[5] Winant, C. D. and Browand, F. K., "Vortex Paring: The Mechanism of Turbulent Mixing-Layer Growth at Moderate Reynolds Number," *Journal of Fluid Mechanics*, Vol. 63, Pt. 2, 1074, pp. 237-255.

[6] Crow, S. C., "Acoustic Gain of a Turbulent Jet," Paper IEG, American Physical Society Meeting, University of Colorado, Boulder, Co., 1972.

[7] Moore, C. J., "The Role of Shear-Layer Instability Waves in Jet Exhaust Noise," *Journal of Fluid Mechanics*, Vol. 80, Pt. 2, 1977, pp. 321-368.

[8] Davies, P.O.A.L., Hardin, J. C., Edwards, A.V.J., and Mason, J. P., "A Potential Flow Model for Calculation of Jet Noise," AIAA Paper 75-441, AIAA 2nd Aero-Acoustics Conference, 1975.

[9] Hardin, J. C. and Mason, J. P., "Broadband Noise Generation by a Vortex Model of Cavity Flow," *AIAA Journal*, Vol. 15, May 1977, pp. 632-637.

[10] Ffowcs Williams, J. E. and Kempton, A. J., "The Noise from the Large-Scale Structure of a Jet," *Journal of Fluid Mechanics*, Vol. 84, Pt. 4, 1978, pp. 637-694.

[11] Liu, J.T.C., "Developing Large-Scale Wave-Like Eddies and the Near Jet Noise Field," *Journal of Fluid Mechanics*, Vol. 62, Pt. 3, 1974, pp. 437-464.

[12] Morris, P. J., "Flow Characteristics of the Large-Scale Wave-Like Structure of a Supersonic Round Jet," *Journal of Sound and Vibration*, Vol. 53, No. 2, 1977, pp. 223-244.

[13] Liu, J.T.C. and Merkine, L., "On the Interaction Between Large-Scale Structure and Fine-Grained Turbulence in a Free Shear Flow. I. The Development of Temporal Interactions in the Mean," *Proceedings of the Royal Society of London, A*, Vol. 352, 1976, pp. 213-247.

[14] Gatski, T. B. and Liu, J.T.C., "On the Interaction Between Large-Scale Structures and Fine-Grained Turbulence in a Free Shear Flow III. A Numerical Solution," *Philosophical Transactions of the Royal Society of London*, to appear.

[15] Lumley, J. L., "Toward a Turbulent Constitutive Relation," *Journal of Fluid Mechanics*, Vol. 41, Pt. 2, 1970, pp. 413-434.

[16] Wygnanski, S. and Fiedler, H. E., "The Two-Dimensional Mixing Region," *Journal of Fluid Mechanics*, Vol. 41, Pt. 2, 1970, pp. 327-361.

[17] Alper, A. and Liu, J.T.C., "On the Interactions Between Large-Scale Structure and Fine-Grained Turbulence in a Free Shear Flow II. The Development of Spatial Interaction in the Mean," *Proceedings of the Royal Society of London, A*, Vol. 359, 1978, pp. 497-523.

[18] Reynolds, W. C. and Hussain, A.K.M.F., "The Mechanics of an Organized Wave in Turbulent Shear Flow, Pt. 3, Theoretical Models and Comparisons with Experiments," *Journal of Fluid Mechanics*, Vol. 54, Pt. 2, 1972, pp. 263-288.

[19] Rotta, J., "Statistische Theorie Nichthomogener Turbulenz," *Zeitschrift fur Physik*, Vol. 129, 1951, pp. 547-572.

[20] Michalke, A., "On the Inviscid Instability of the Hyperbolic Tangent Velocity Profile," *Journal of Fluid Mechanics*, Vol. 19, 1964, pp. 543-556.

[21] Goldstein, M. E., *Aeroacoustics*, McGraw Hill, New York, 1976, pp. 180-191.

[22] Crow, S. C., "Aerodynamic Sound Emission as a Singular Perturbation Problem," *Studies in Applied Mathematics*, Vol. 49, 1970, pp. 21-44.

[23] Ribner, H. S., "The Generation of Sound by Turbulent Jets," *Advances in Applied Mechanics*, Vol. 8, Academic Press, New York, 1964, pp. 103-182.

[24] Michalke, A., "Sound Generation by Amplified Disturbances in Free Shear Layers," German Air and Space Travel Research Rept. 69-90, 1969.

[25] Powell, A., "Theory of Vortex Sound," *The Journal of the Acoustical Society of America*, Vol. 36, No. 1, 1964, pp. 177-195.

[26] Hardin, J. C., "Noise Calculation on the Basis of Vortex Flow Models," *ASME Symposium on Noise and Fluids Engineering*, Atlanta, Ga., 1977.